Available online at www.sciencedirect.com
SCIENCE DIRECT®
Computers and Structures 82 (2004) 627–637
Computers & Structures
www.elsevier.com/locate/compstruc

Numerical analysis of multi-layer composite plates with internal delamination

L.H. Yam *, Z. Wei, L. Cheng, W.O. Wong

Department of Mechanical Engineering, The Hong Kong Polytechnic University, Hung Hom, Kowloon, Hong Kong

Received 5 February 2003; accepted 17 December 2003

Abstract

A three-dimensional finite element model for the delaminated fiber reinforced composites is proposed to analyze the dynamics of multi-layer composite plates with internal delamination. Virtual elements are adopted in the region of delamination to prevent element penetration. Natural frequency, modal displacement and modal strain are analyzed for samples with different dimensions of delamination. Numerical results show a good agreement with the available experimental data and an enhancement of the accuracy of the results when the proposed model is adopted. The results of this study are useful for detecting delamination in multi-layer composite materials.

Keywords: Multi-layer composites; Finite element model; Virtual elements; Internal delamination; Modal parameters; Numerical analysis

1. Introduction

The use of composite materials in space vehicles and various machine components has increased considerably over the past decades. Under repeated or impact loads these materials are subjected to various forms of damage, mostly delaminations and cracks [1–4]. Such damage becomes an obstacle to the more extensive usage of composite materials. Therefore, the monitoring of internal or hidden damage in composite material is critical in engineering practice [5]. The use of vibration-based techniques as nondestructive testing methods for damage monitoring of laminated composite is a field attracting the interest of many researchers [6–12].

The effective damage monitoring for this kind of material or structure depends largely on the accurate prediction or estimation of mechanical or dynamic behaviors of both intact and damaged composite materials [13]. As it is difficult to obtain accurate analytical solution for multi-layer material problem theoretically, the computational approach, e.g., finite element method, plays an important role in the implement of damage detection for laminated composites. There are contributions on both numerical and experimental investigations into the behavior of delaminated multi-layer composites [14–19].

After Sankar [20] had modeled a delaminated beam as two sublaminates by offset beam finite elements, Rikards [21] developed a model of finite superelements for sandwich composite beam and plate without delamination, each layer being considered as a simple Timoshenko beam. Later, Gabelrab [3] discussed the modal variation of delaminated beam for different boundary conditions and Ousset and Roudolff [4] analyzed the delaminated multi-layer composite plate based on Mindlin Reissner plate model. Zak et al. [22] and Ousset and Roudolff [4] developed models of finite elements for beams and plates with boundary delamination. Among most of the publications the prediction of material mechanical or dynamic behaviors is based on the classical laminated plate theory [23]. Due to the ignorance of

* Corresponding author. Tel.: +852-2766-7820; fax: +852-2365-4703.
E-mail address: mmlhyam@polyu.edu.hk (L.H. Yam).

0045-7949/$ - see front matter
doi:10.1016/j.compstruc.2003.12.003

the transverse shear deformation effect, the classical layerwise theory based on the straight normal assumption of elastic thin plate cannot provide accurate results for moderately thick laminated plates, for which the in-plane elastic modulus is much higher than the transverse shear modulus [24]. Besides, the Poisson's effect is significant for angle-ply laminated plates. Therefore, three-dimensional layerwise theory must be adopted in order to obtain an accurate prediction of dynamic response for multi-layer composite plates. In addition, potential dangers are often induced by hidden or internal delaminations in the in-service laminated composites. However, there is a lack of both numerical and experimental investigations on internal delaminations with different geometries in laminated composites.

In this paper, a three-dimensional finite element model for multi-layer composites with internal delamination is established, and the fiber orientation of individual lamina as well as the transverse shear effect are taken into account. Numerical calculation is carried out for different plates. Natural frequencies, modal displacements and strains of the intact and damaged multi-layer composite plates are subsequently analyzed for various samples.

2. Three-dimensional elastic theory for laminated composite plates

2.1. Geometric equation

By introducing a Cartesian global coordinate system x, y, z to a rectangular plate with uniform thickness as shown in Fig. 1, the displacements of a point (x,y,z) in the plate can be expressed as

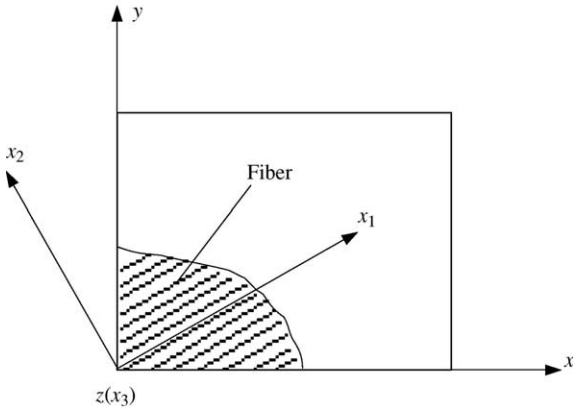

Fig. 1. The cross-ply laminated plate and the coordinate systems.

$$\{u\} = (u_1, u_2, u_3)^{\mathrm{T}} = (u(x,y,z), v(x,y,z), w(x,y,z))^{\mathrm{T}} \quad (1)$$

where u, v and w represent the displacements along x, y and z axes, respectively.

The linear strain–displacement relationships are

$$\varepsilon_{ij} = \tfrac{1}{2}(u_{i,j} + u_{j,i}) \quad (i,j = 1,2,3) \quad (2)$$

2.2. Physical equation

Assume that the individual lamina is orthotropic with fiber orientation along x_1 axis of the Cartesian coordinate system x_1, x_2, x_3 (local material coordinates) as shown in Fig. 1, the constitutive equation for the lamina is

$$\{\sigma^*\} = [C]\{\varepsilon^*\} \quad (3)$$

where

$$\{\sigma^*\} = (\sigma^*_{11}, \sigma^*_{22}, \sigma^*_{33}, \sigma^*_{23}, \sigma^*_{13}, \sigma^*_{12})^{\mathrm{T}} \quad \text{and}$$
$$\{\varepsilon^*\} = (\varepsilon^*_{11}, \varepsilon^*_{22}, \varepsilon^*_{33}, \varepsilon^*_{23}, \varepsilon^*_{13}, \varepsilon^*_{12})^{\mathrm{T}}$$

are vectors of stress and strain along the main directions in local coordinate system, respectively. $[C]$ is the elastic constant matrix of the material expressed as

$$[C]^{-1} = \begin{bmatrix} \frac{1}{E_1} & \frac{-v_{12}}{E_1} & \frac{-v_{13}}{E_1} & 0 & 0 & 0 \\ \frac{-v_{12}}{E_1} & \frac{1}{E_2} & \frac{-v_{23}}{E_2} & 0 & 0 & 0 \\ \frac{-v_{13}}{E_1} & \frac{-v_{23}}{E_2} & \frac{1}{E_3} & 0 & 0 & 0 \\ 0 & 0 & 0 & \frac{1}{G_{23}} & 0 & 0 \\ 0 & 0 & 0 & 0 & \frac{1}{G_{13}} & 0 \\ 0 & 0 & 0 & 0 & 0 & \frac{1}{G_{12}} \end{bmatrix} \quad (4)$$

E_1, E_2, E_3, G_{12}, G_{13}, G_{23}, v_{12}, v_{13} and v_{23} are the orthotropic elastic constants of the lamina.

The stresses in the global coordinate system can be obtained as follows:

$$\{\sigma\} = (\sigma_{xx}, \sigma_{yy}, \sigma_{zz}, \sigma_{yz}, \sigma_{xz}, \sigma_{xy})^{\mathrm{T}} = [A]\{\sigma^*\} \quad (5)$$

where $[A]$ is the matrix of directional cosines relevant to coordinate transformation from local material coordinates to the global ones, i.e.

$$[A] = \begin{bmatrix} \cos^2\theta & \sin^2\theta & 0 & 0 & 0 & -2\sin\theta\cos\theta \\ \sin^2\theta & \cos^2\theta & 0 & 0 & 0 & 2\sin\theta\cos\theta \\ 0 & 0 & 1 & 0 & 0 & 0 \\ 0 & 0 & 0 & \cos\theta & \sin\theta & 0 \\ 0 & 0 & 0 & -\sin\theta & \cos\theta & 0 \\ \sin\theta\cos\theta & -\sin\theta\cos\theta & 0 & 0 & 0 & \cos^2\theta - \sin^2\theta \end{bmatrix} \quad (6)$$

Therefore, the constitutive equation in the global coordinate system can be expressed as

$$\{\sigma\} = [A][C][A]^{-1}\{\varepsilon\} \quad (7)$$

where

$$\{\varepsilon\} = (\varepsilon_{xx}, \varepsilon_{yy}, \varepsilon_{zz}, \varepsilon_{yz}, \varepsilon_{xz}, \varepsilon_{xy})^{\mathrm{T}}$$

is the strain vector in the global coordinate system x, y, z.

3. Finite element modeling

3.1. Element model description

The finite element used for multi-layer plate dynamic behavior analysis is a kind of eight-node rectangular thin plate element as shown in Fig. 2. For each node, there are three degrees of freedom, i.e., translations along x, y and z axes. The element thickness is assigned to be equal to that of the corresponding individual lamina, which may not be the same for all the elements. The element coordinate system is arranged such that the first axis is coincident with the fiber direction. All physical parameters throughout an element are assumed to be the same.

3.2. Expressions for displacement and strain

For an eight-node finite element with three degrees of freedom per node, the displacement field over an element is given by

$$\{u\} = \sum_{i=1}^{8} [N_i]\{\delta_i\} \tag{8}$$

where

$$\{\delta_i\} = (u_i, v_i, w_i)^{\mathrm{T}}$$

is the displacement vector at node i and

$$[N_i] = N_i[I_3]$$

where $[I_3]$ is a three-order unit matrix and N_i the shape function for node i [25]. Then the strain of each element can be expressed in terms of displacement in the global coordinate system as

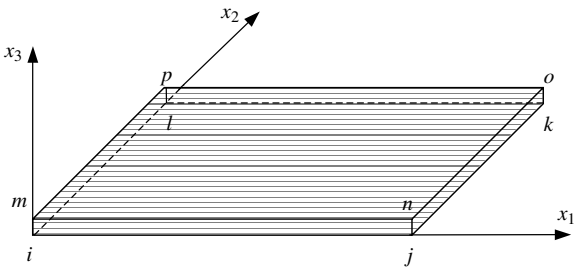

Fig. 2. The eight-node thin plate element and the local coordinate system.

$$\{\varepsilon^e\} = \sum_{i=1}^{8} [B_i]\{\delta_i\} \tag{9}$$

where

$$[B_i] = [\Delta][N_i] \tag{10}$$

and

$$[\Delta] = \begin{bmatrix} \frac{\partial}{\partial x} & 0 & 0 \\ 0 & \frac{\partial}{\partial y} & 0 \\ 0 & 0 & \frac{\partial}{\partial z} \\ 0 & \frac{\partial}{2\partial z} & \frac{\partial}{2\partial y} \\ \frac{\partial}{2\partial z} & 0 & \frac{\partial}{2\partial x} \\ \frac{\partial}{2\partial y} & \frac{\partial}{2\partial x} & 0 \end{bmatrix} \tag{11}$$

Thus, for a given element, the strain can be expressed in terms of nodal displacements as

$$\{\varepsilon^e\} = [B]\{\delta^e\} \tag{12}$$

where

$$[B] = [[B_1], [B_2], \ldots, B_8]]$$

and

$$\{\delta^e\} = (\{\delta_1\}^{\mathrm{T}}, \ldots, \{\delta_8\}^{\mathrm{T}})^{\mathrm{T}}.$$

3.3. Stress–strain relationship and equation of motion

According to Eqs. (7) and (12), the stresses of an element in the global coordinate system can be expressed by the nodal displacements as

$$\{\sigma^e\} = [A][C][A]^{-1}[B]\{\delta^e\} \tag{13}$$

Thus, the element stiffness matrix may be written as

$$[K^e] = \int_{V_e} [B]^{\mathrm{T}}[A][C][A]^{-1}[B]\,\mathrm{d}V \tag{14}$$

Then, the strain energy of the kth element is

$$U_k^e = \frac{1}{2}\int_{V_k} \{\varepsilon^e\}^{\mathrm{T}}\{\sigma^e\}\,\mathrm{d}V = \frac{1}{2}\{\delta_k^e\}^{\mathrm{T}}[K_k^e]\{\delta_k^e\} \tag{15}$$

where $\{\delta_k^e\}$ represents the displacement vector of the kth element. The total strain energy for a composite plate consisting of N elements can be expressed as

$$U = \sum_{k=1}^{N} U_k^e = \frac{1}{2}\sum_{k=1}^{N} \{\delta_k^e\}^{\mathrm{T}}\{\delta_k^e\}^{\mathrm{T}}[K^e]\{\delta_k^e\} \tag{16}$$

Therefore, after assembly of nodal displacements of all elements, the total strain energy of a multi-layer composite plate can be represented as

$$U = \tfrac{1}{2}\{\delta\}^{\mathrm{T}}[K]\{\delta\} \tag{17}$$

where $\{\delta\}$ and $[K]$ are the global nodal displacement vector and stiffness matrix, respectively.

Similarly, if the composite plate experiences a harmonic motion with angular frequency ω, the kinetic energy of the composite plate will be

$$T = \tfrac{1}{2}\omega^2\{\delta\}^{\mathrm{T}}[M]\{\delta\} \tag{18}$$

where $[M]$ is the global mass matrix. Then, using the Lagrange's principle the equation of motion for free vibration of the composite plate is reduced to the eigenvalue problem of

$$([K] - \omega^2[M])\{\delta\} = 0. \tag{19}$$

3.4. Continuity between adjacent laminas and delamination description

For an arbitrary laminated plate with an internal delamination as shown in Fig. 3, suppose that the delamination region is between two separate sublaminates called the upper and lower sublaminates, respectively. To ensure the material continuity, displacements and their variations of each pair of coincident nodes on any two upper and lower adjacent laminas have to be equal except those in the delaminated region.

To simulate the actual status of delamination, an extremely thin layer is inserted between the upper and lower sublaminates within the delaminated region. When the plate is in motion, it is physically impossible that elements of the upper and lower sublaminates penetrate into each other within the delamination region. Therefore, virtual elements are inserted between the penetrated nodes of the upper and lower sublaminates within the delaminated region to ensure a reasonable deformation without penetration.

Virtual/artificial spring elements have been previously used to simulate various conditions of structures [26] and the mechanical coupling between different components [27,28]. Further studies extended their use to vibroacoustic systems in which a structure is coupled to an acoustic medium [29]. This technique is used here to bring desirable effect to the interface in the delaminated region. Every inserted virtual element is a spring with a stiffness constant k_r. The local and global

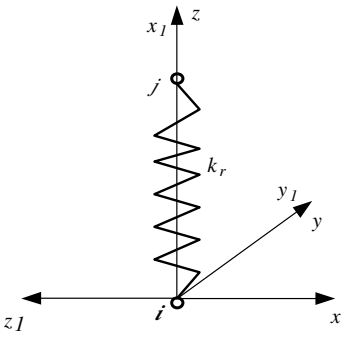

Fig. 4. Virtual spring element and the coordinate systems.

coordinate systems are x_1, y_2, z_3 and x, y, z, respectively as shown in Fig. 4. If the displacements of nodes i and j are u_i, v_i, w_i and u_j, v_j, w_j, respectively, in the global coordinates the components of the distance change between the two nodes of a virtual element are expressed in terms of nodal displacements as

$$\{\delta_r\} = (u_j - u_i, v_j - v_i, w_j - w_i)^{\mathrm{T}} = [B_r]\{\delta^e\} \tag{20}$$

where

$$[B_r] = \begin{bmatrix} -1 & 0 & 0 & 1 & 0 & 0 \\ 0 & -1 & 0 & 0 & 1 & 0 \\ 0 & 0 & -1 & 0 & 0 & 1 \end{bmatrix}$$

The internal spring force can be expressed as

$$\{N_r\} = (N_{rx}, N_{ry}, N_{rz})^{\mathrm{T}} = [A_r][K_r][A_r]^{-1}\{\delta_r\} \tag{21}$$

where

$$[K_r] = \begin{bmatrix} k_r & 0 & 0 \\ 0 & 0 & 0 \\ 0 & 0 & 0 \end{bmatrix} \tag{22}$$

is the local stiffness matrix of the spring with constant k_r, and

$$[A_r] = \begin{bmatrix} 0 & 0 & -1 \\ 0 & 1 & 0 \\ 1 & 0 & 0 \end{bmatrix}$$

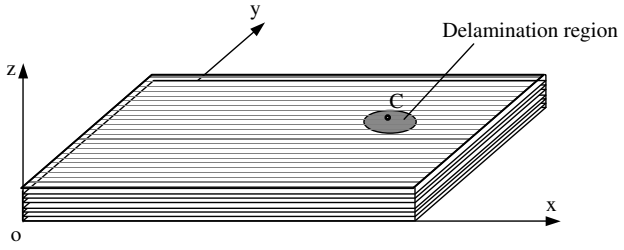

Fig. 3. Geometry of multi-layer composite plate with local internal delamination.

is the transformation matrix between the global and local coordinate systems.

Let

$$[D_r] = [A_r][K_r][A_r]^{-1}$$

the nodal forces of the virtual element can be expressed as

$$\{F_r\} = (F_{rx}, F_{ry}, F_{rz})^{\mathrm{T}} = [B_r]^{\mathrm{T}}[D_r][B_r]\{\delta^e\}$$

Hence the stiffness matrix of the virtual element is

$$[K_r^e] = [B_r]^{\mathrm{T}}[D_r][B_r] \tag{23}$$

The spring constant k_r in Eq. (22) will be so selected that the upper and lower parts within the delaminated region can keep a reasonable gap or contact without penetration when the plate is in motion. It will be discussed later.

4. Numerical examples and results

The proposed finite element formulation is then incorporated into a finite element analysis computer program for validation. Some examples are investigated numerically to analyze the variation of the natural frequencies and modal displacements and modal strains induced by delamination.

4.1. Sample description

The samples for numerical simulation are multi-layer square plates composed of different fiber reinforced laminae with four edges free. Assume that all samples are orthotropic.

Three types of laminated composite plates are considered in this study. Plate 1 is an 8-layer CFRP square plate with a side length of 178 mm and a thickness of 1.58 mm. All the ply orientations are equal to 0° and the material constants are $E_1 = 172.7$ GPa, $E_2 = E_3 = 7.2$ GPa, $G_{12} = G_{13} = 3.76$ GPa, $G_{23} = 2.71$ GPa, $v_{12} = v_{13} = 0.3$, $v_{23} = 0.33$ and $\rho = 1566\ \mathrm{kg\,m^{-3}}$.

Plate 2 is a 12-layer GFRP square laminated plate with a side length of 204.6 mm and a thickness of 2.11 mm. The ply orientation distribution along the plate thickness is $(0°/-60°/60°/0°/-60°/60°)_s$ and the material constants are $E_1 = 37.78$ GPa, $E_2 = E_3 = 10.9$ Pa, $G_{12} = G_{23} = G_{13} = 4.91$ GPa, $v_{12} = v_{13} = 0.3$, $v_{23} = 0.11$ and $\rho = 2003.5\ \mathrm{kg\,m^{-3}}$.

Plate 3 is an 8-layer GFRP rectangular square laminated plate with a side length of 225.5 mm and a thickness of 2.05 mm. The ply orientation distribution along the plate thickness is (0°/90°/0°//90°/90°/0°/90°/0°), where the '//' denotes the location of delamination as shown in Fig. 3. The interspace between the upper and lower sublaminates is assumed as 10^{-3} mm within the delaminated region. The material constants are the same as those of Plate 2 except that $\rho = 1813.9\ \mathrm{kg\,m^{-3}}$. The center of the delamination region is located at point C with coordinates $x = 169.125$ mm, $y = 169.125$ mm and $z = 1.28125$ mm.

4.2. Results and discussions

4.2.1. Natural frequencies for plates without delamination

FE discretization effect is one of the dominant factors for result accuracy of computation. For the special structure used as the sample each lamina is meshed the same as each other, i.e. the element area is foursquare and the thickness is equal to that of the lamina. Table 1 shows the computation results of natural frequencies for

Table 1
Natural frequencies of the intact plates for different meshes (Hz)

Mode	Element number for each lamina				
	4	25	100	400	900
Plate 1					
1	85.94	83.37	82.50	82.26	82.22
2	130.58	120.52	116.39	113.10	114.70
3	217.04	219.99	211.90	207.29	208.32
4	417.07	373.08	333.16	325.28	326.08
5	729.89	503.21	449.33	408.51	407.64
6	765.70	667.43	571.10	539.92	539.06
Plate 2					
1	97.56	96.58	95.78	95.66	95.62
2	174.70	154.81	153.04	152.53	152.47
3	278.83	247.23	240.57	238.74	239.13
4	305.11	261.72	258.99	258.03	257.72
5	328.38	310.92	278.61	277.50	277.35
6	521.88	513.10	498.02	496.54	497.01

Table 2
Natural frequencies of the intact plates for different methods (Hz)

Mode	Plate 1			Plate 2		
	Present	Reference [30]		Present	Reference [30]	
		Numerical	Experimental		Numerical	Experimental
1	82.26	83.57	81.5	95.66	108.17	90.4
2	113.10	118.42	107.4	152.53	168.64	144.7
3	207.29	207.79	196.6	238.74	218.64	222.3
4	325.28	329.41	285.5	258.03	280.15	264.1
5	408.51	419.83	382.5	277.50	301.00	281.1
6	539.92	546.93	531	496.54	505.15	492.6

Plates 1 and 2 for different meshes for one lamina. It is seen that the results converge after each lamina is discretized by 400 or more elements. Therefore, in order to save CPU time, 400 elements are adopted for each lamina in the subsequent computations except that the delamination region is fractionized.

Table 2 shows the natural frequencies of the first six modes for bending vibration of Plates 1 and 2 while the referential numerical and experimental results from Ref. [30] are also listed for comparison. It demonstrates a better agreement between the present results and the experimental results in Ref. [30].

4.2.2. Effect of spring constant on natural frequency

The distance change of the adjacent points just above and below the delamination region may be different if the value of k_r in Eq. (22) varies for the delaminated plate. In fact, the virtual spring with certain stiffness can introduce additional constraint, which may result in increase of vibration frequency [26–28]. Without such inserted virtual spring elements, the movements of nodes on the free surface of the delamination will not be restricted. With nearly complete restriction, i.e. the spring constant of the virtual element being extremely large (e.g. larger than 10^6 N m^{-1}), the natural frequencies of the plate will increase significantly especially for high modes with large delamination.

Fig. 5 shows the displacements of the upper and lower points within the delaminated region for the first 10 modes for Plate 3 with delamination areas of 165 and 2475.5 mm^2, respectively, when the virtual spring element is not inserted. The names and locations of the above points are listed in Table 3. It is apparent that penetration between the upper and lower parts within the delaminated region occurs in modes 6 and 7 when delamination area is 165 mm^2, and for the case of delamination area 2475.5 mm^2 penetration is obviously seen in the sixth, seventh and ninth modes.

Further numerical simulation for Plate 3 with the delamination areas of 165 and 2475.5 mm^2 shows that when k_r is larger than 0.1 N m^{-1} the upper and lower sublaminates in the delamintion region do not penetrate

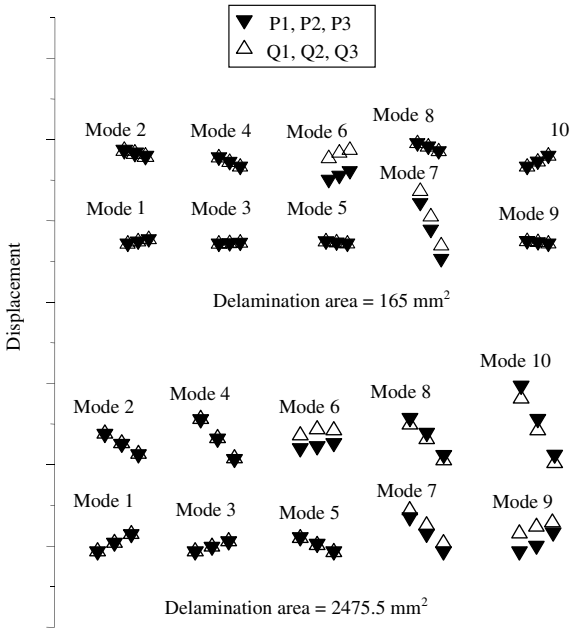

Fig. 5. Maximum displacements of selected points for the first 10 modes of Plate 3 without virtual spring within the delaminated region.

into each other for the above three modes when the plate is in motion. Variations of natural frequencies with different values of k_r are shown in Table 4 for the first 10 modes of Plate 3 with the delamination area of 2475.5 mm^2. It is seen that the spring-induced increase of frequency is not significant when the spring constant is less than 10^3 N m^{-1}. Fig. 6 shows the decreases of natural frequencies of the first 15 modes for Plate 3 with different delamination areas without the virtual spring elements in the delaminated region. Table 5 shows the influence of spring constant on natural frequencies of the sixth, seventh and ninth modes for Plate 3 with different delamination areas when $k_r = 10^6$ N m^{-1}.

A combination of comparison between Fig. 5 and Table 5 with Table 4 reveals that the effect of the spring

Table 3
Points and their locations for computation of displacements as shown in Fig. 5

Point name	Description	Coordinate (mm)		
		x	*y*	*z*
P1	On bottom surface of the upper sublaminate	164	56.375	1.28125
P2		169.125	56.375	1.28125
P3		174.25	56.375	1.28125
Q1	On top surface of the lower sublaminate	164	56.375	*1.28025*
Q2		169.125	56.375	*1.28025*
Q3		174.25	56.375	1.28025

Table 4
Natural frequency increases with virtual spring constants for Plate 3 with delamination area of 2475.5 mm^2 (Hz)

Mode	Spring constant k_r (N m^{-1})					
	10^{-2}	10^{-1}	10^{2}	10^{3}	10^{5}	10^{7}
1	0	0	0	0	0.001	0.003
2	0	0	0	0	0.01	0.07
3	0	0	0	0	0.01	0.2
4	0	0	0	0	0.1	0.63
5	0	0	0	0	0.07	0.49
6	0	0	0	0	0.03	0.17
7	0	0	0	0.01	0.12	0.69
8	0	0	0	0	0.2	1.59
9	0	0	0	0	0.1	1.02
10	0	0	0	0	1.04	6.1

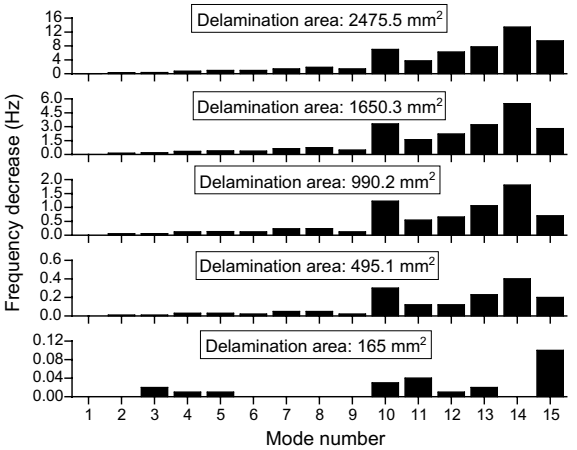

Fig. 6. Natural frequency decreases with delamination areas for Plate 3 without virtual spring elements.

constant on natural frequency increases with the delamination area and becomes relatively remarkable when the value of k_r goes up. Therefore, virtual spring elements with spring constant $k_r = 10^{-1}$ N m^{-1} are adopted for numerical computation of modes 6, 7 and 9 of the delaminated plates. The variations of natural frequencies with the delamination areas are listed in Table 6 for the above three modes when k_r is 10^{-1} N m^{-1}. It is seen that although the effect of virtual spring element increases when the delamination grows, but it is not as significant as that of delamination.

4.2.3. Effect of delamination area on natural frequencies

The effect of delamination area on natural frequencies of the multi-layer composite plate is studied numerically for Plate 3. As shown in Fig. 3, the delamination region is assumed elliptic with center *C*. From Fig. 6 and Table 6, it can be seen that the natural frequency decreases with the increase of delamination area. The only exception occurs when the delamination area is 165 mm^2 (the smallest area for analysis) for mode 6. This may be caused by the introduction of the virtual spring elements because the location of the delamination is just near the peak of mode shape for mode 6 as shown in Fig. 7. But even in this case the percentage change of natural frequency is less than 0.05%. Therefore errors introduced by the virtual element will not become a menace in study on delamination-induced variations of other parameters more applicable than frequency, such as displacement and strain.

Table 5
Natural frequency decreases with delamination areas for Plate 3 with virtual elements of spring constant $k_r = 10^6$ N m^{-1}

Mode	Delamination area (mm^2)				
	165.0	495.1	990.2	1650.3	2475.5
6	−0.21	0.02	0.11	0.33	0.81
7	0	0.05	0.22	0.61	0.9
9	0	0.02	0.12	0.43	0.83

Table 6
Natural frequency decreases of Plate 3 with different dimensions of delaminations and virtual elements of spring constant $k_r = 0.1$ N m^{-1} (Hz)

Mode	Delamination area (mm^2)				
	165.0	495.1	990.2	1650.3	2475.5
6	−0.21	0.02	0.11	0.36	0.92
7	0	0.05	0.23	0.62	1.38
9	0	0.02	0.13	0.48	1.37

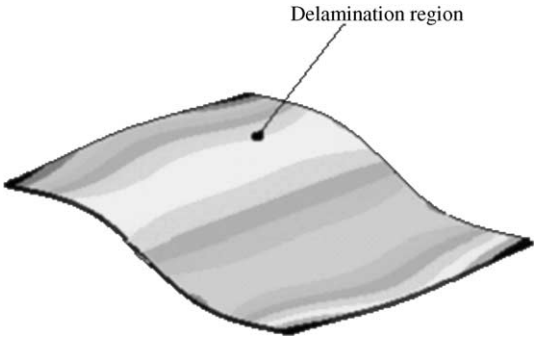

Fig. 7. The sixth displacement mode shape for Plate 3.

From Fig. 6 and Table 6, it can be seen that the natural frequency generally decreases with the increase of delamination area. The only exception occurs when the delamination area is 165 mm^2 (the smallest area to be analyzed) for mode 6. This may be caused by the introduction of the virtual spring elements because the location of the delamination is very near the peak of mode shape for mode 6 as shown in Fig. 7. However, even in this case the percentage change of natural frequency is less than 0.05%. Therefore, errors introduced by the virtual elements cannot become a menace in study on delamination-induced variations of other parameters more applicable than frequency, such as displacement and strain.

Fig. 6 and Table 6 show that delamination with small area has very little influence on natural frequencies for all computed modes. The average percentage change of natural frequencies is only about 0.066% when the delamination area reaches 990.2 mm^2, and even the maximum value is about 0.18% for mode 10. A similar variation pattern is also seen when the delamination area increases gradually. The frequency changes are greater than 1% for modes 11 and 12, and the maximum is about 1.16% for the fifth mode when the delamination area is 2475.5 mm^2. This implies that the natural frequency is not sensitive to delamination for multi-layer composite plates.

The above results show that the influence of delamination on natural frequency varies with vibration modes, and this phenomenon may be useful to determine the location or area of delamination. However, this is basically impracticable, because, the experimental equipment can hardly extract modes higher than 10 for composite plates, and it is difficult to measure the small delamination-induced change of frequency.

If internal delamination occurs in the vibrating plate, there may be interactive motion or impact between the upper and lower sublaminates within the delamination region. Further investigation on the local displacements of the plate shows that the differences of displacements between the points just on the upper and lower surfaces of the delamination region vary with modes. The relative displacements in x–y plane are also larger in some modes than in other modes, i.e., the interactive motion between the upper and lower surfaces within the delamination region occurs when the plate vibrates. Thus, when internal delamination occurs somewhere in a composite plate, there may be interactive motion or impact within the delamination region during vibration of the plate. These phenomena cause the variations of energy dissipation in the plate. Hence, the variation of energy dissipation in the plate during vibration can be the hint for delamination detection. Therefore, the relative displacement in z direction within the delamination region is restricted using virtual spring to avoid the physically impossible penetration, and the selection of k_r with respect to the transverse properties of the orthotropic lamina is not necessary.

4.2.4. Variation of displacement and strain due to delamination of the vibrating composite plate

Analysis of modal parameters is known as one of the practical experimental methods for damage detection. As delamination of multi-layer composites means local structural change, it can, to some extent, induce variations of vibration responses. To investigate the delamination-dependent vibration responses the changes of modal deformation have been computed for delaminated composite of Plate 3. For the first 15 modes the modal displacements along z-direction and modal strains along x-direction and y-direction are computed respectively at some concerned points.

For the first 15 modes, displacements and strains are computed at the point with the same x and y coordinates as those of point C as shown in Fig. 3, and $z = 2.05$ mm, i.e. the point on the top free surface of Plate 3. Fig. 8 shows the results of relative changes of frequencies, peak displacements and strains when the delamination area is 165.0 mm^2 for Plate 3. In the table w_m represents the unit-normalized displacement along z axis at the considered point.

Fig. 8 shows that delamination-induced changes of displacement and strain are much greater than that of frequency. The changes of displacement and strain are more remarkable in the third, fifth, sixth and seventh modes than those in other modes. Both the most remarkable changes of displacement and strain appear in the same mode—the third mode. It should be noted that the most remarkable decrease of frequency also occurs in the third mode for the computed case. From the third mode shape of Plate 3 as shown in Fig. 9, it is noted that the delamination is close to the region of plate displacements transition from positive to negative.

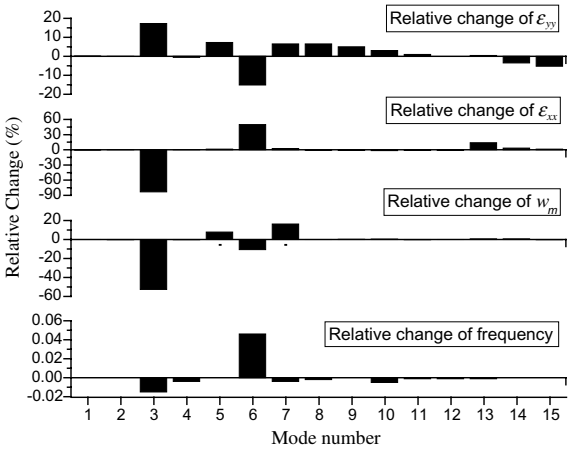

Fig. 8. Relative changes of modal parameters at a point on top surface just above the center of the delamination region for Plate 3 with a delamination area of 165.0 mm^2.

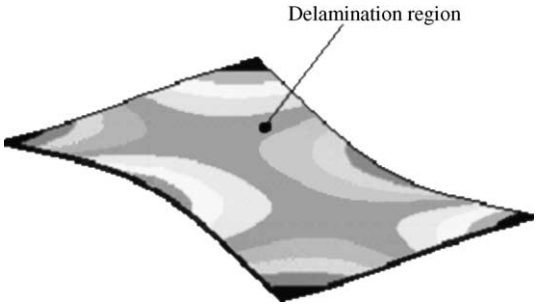

Fig. 9. The third displacement mode shape for Plate 3.

Table 7
Relative changes of displacements and strains at the points with the maximum displacements on top surface for Plate 3 with a delamination area of 165.0 mm^2

Mode	Coordinate of point for computation (mm)			Relative change of w_m (%)	Relative change of ε_{xx} (%)	Relative change of ε_{yy} (%)
	x	y	z			
1	0	0	2.05	−0.02	−0.051	−0.049
2	112.75	225.5	2.05	0	0.119	0.123
3	225.5	225.5	2.05	0.001	−13.488	−1.085
4	225.5	0	2.05	0	0.388	0.204
5	0	225.5	2.05	−1.929	−1.543	−1.061
6	225.5	0	2.05	−14.081	−19.229	−7.27
7	0	66.625	2.05	−13.154	−15.299	−5.614
8	0	10.25	2.05	−0.665	0.183	−0.219
9	225.5	0	2.05	−0.001	−0.384	−0.291
10	112.75	0	2.05	−0.051	0.134	0.127
11	0	112.75	2.05	0	−0.109	−0.111
12	30.75	0	2.05	−0.27	−0.062	−0.064
13	225.5	225.5	2.05	0	0.036	0.522
14	225.5	153.75	2.05	−0.714	0.04	0
15	112.75	0	2.05	0.001	0	−0.217
Average of absolute values				2.059	3.404	3.131

In order to investigate the local variation of deformation induced by delamination, changes of displacements and strains at another point are computed for the considered modes. Table 7 shows the relative changes of displacements and strains at the point with the maximum displacement on the top surface of Plate 3 before delamination. It can be seen that unlike the results in Fig. 8, neither the displacement change nor the strain change is the largest for the third mode although this point (with coordinates 225.5, 225.5, 2.05) in Table 7 is not far away from the point, the results of which are shown in Fig. 8.

Therefore, the influence of delamination on deformation of a composite plate is dependent on modes. It is an effective method to detect damage by investigation into damage-induced local changes of structural geometric, physical and mechanical parameters by means of displacement and strain measurement with consideration of natural frequency change. In fact, experimental modal strain analysis has already been proved as reasonable and practical for investigation of local variation of structural parameters [31].

5. Conclusions

The delamination problem for multi-layer composite plates has been analyzed using finite element method and modal analysis. To achieve accurate results for delamination detection of multi-layer composite plate, different fiber orientations, orthotropy of laminated composites and transverse shear effect are taken into account in the finite element computation. For practical nondestructive damage detection, internal elliptic delamination is considered and virtual interface elements are introduced to simulate local delamination and to prevent physically impossible penetration. The following conclusions may be drawn from the results of numerical simulation in this study.

(a) The finite element model proposed in this paper can predict accurately the dynamic behaviors of a multi-layer composite plate with internal delamination at arbitrary location. It is not as computationally expensive as the usually used three-dimensional brick elements when the proposed element is used because there is no restriction of ratio between element length and thickness. The virtual element with very small spring constant has very slight influence on natural frequencies and mode shapes of the computed plates but can successfully prevent physically impossible penetration of the upper and lower parts within the delaminated region.
(b) Local internal delamination has slight effect on natural frequencies of a multi-layer composite plate although the extent of natural frequency variation increases with both the delamination dimension and the order of natural frequency.
(c) Delamination-induced change of deformation is more sensitive than that of frequency, and changes of both displacement and strain are mode-dependent. The most remarkable delamination-induced changes of displacement and strain occur in the same mode as the most remarkable decrease of frequency when the delamination area is relatively small for the cases considered in this paper.
(d) The results of numerical analysis in this study can be taken as guidance for arrangement of displacement and strain measurements on the surface of specimen when experimental modal analysis is carried out to investigate local changes of structural parameters for damage detection. The finite element model, strategy and numerical method provided in this paper can be used for dynamic response analysis of damaged engineering structures, especially for multi-layer composite plates.
(e) If the layers are also damaged, for example cracks occur in a laminar, the damage in the related elements must be considered via describing the variation of material elastic parameters. In this case, the elastic matrix of damaged element is not the same as that of the intact one. By introducing special variables into the elastic matrix to indicate the damage features, the dynamic behaviors of the damaged composites can be computed, and the damage-induced variations of modal parameters can then be investigated for damage detection. This topic is also under research in our project.

Acknowledgements

The work described in this paper has been supported by the Research Grants Council of Hong Kong Special Administrative Region, China (Project no. PolyU 5174/01E and PolyU 5313/03E). The authors are also grateful for the support of The Hong Kong Polytechnic University in carrying out this project.

References

[1] Tsai SW, Hann HT. Introduction to composite materials. Westport, Connecticut: Technic Publishing Company; 1980.
[2] Voyiadjis GZ. Damage in composite materials. Amsterdam, New York: Elsevier; 1993.
[3] Gadelrab RM. The effect of delamination on the natural frequencies of a laminated composite beam. J Sound Vib 1996;197(3):283–92.
[4] Osset Y, Roudolff F. Numerical analysis of delamination in multi-layered composite plates. Comput Mech 2000; 20(1/2):122–6.

[5] Gerardi TG. Health monitory aircraft. J Intell Mater Syst Struct 1990;1:375–85.
[6] Salawu OS. Detection of structural damage through changes in frequency: a review. Eng Struct 1997;19:718–23.
[7] Rytter A, Kirkegaard PH. Vibrational-based inspection of a steel mast. In: Proceedings of the 12th International Modal Analysis Conference, Hawaii, 1994. p. 1602–8.
[8] Gomes AJMA, Silva JMME. On the use of modal analysis for crack identification. In: Proceedings of the 8th International Modal Analysis Conference, FL USA, 1991. p. 1108–15.
[9] Cawley P, Adams RD. The location of defects in structure from measurements of natural frequencies. J Strain Anal 1979;4:49–57.
[10] Sanders D, Kim YI, Stubbs RN. Non-destructive evaluation of damage in composite structures using modal parameters. Exp Mech 1992;32:240–51.
[11] Ceravolo R, Stefano AD. Damage location in structure through a connectivistic use of FEM modal analyses. Int J Anal Exp Modal Anal 1995;10(3):178–86.
[12] Crema LB, Mastroddi F. Frequency-domain based approaches for damage detection and localisation in aeronautical structure. In: Proceedings of the International Modal Analysis Conference, 1995. p. 1322–30.
[13] Tappet PM, Snyder TD, Robertshaw HH. Attacking the damage identification problem. In: Proceedings of SPIE—The International Society for Optical Engineering Smart Structures and Materials: Smart Sensing, Processing and Instrumentation 2443, 1995. p. 286–294.
[14] Raghuram PV, Murty AVK. A high precision coupled bending-extension triangular finite element for laminated plates. Comput Struct 1999;72(6):763–77.
[15] Lee J. Free vibration analysis of delaminated composite beams. Comput Struct 2000;74(2):121–9.
[16] Rikards R. Interlaminar fracture behaviour of laminated composites. Comput Struct 2000;76(1–3):11–8.
[17] Borovkov A, Palmov V, Banichuk N, Saurin V, Barthold F, Stein E. Macro-failure criterion for the theory of laminated composite structures with free edge delaminations. Comput Struct 2000;76(1–3):195–204.
[18] Lingen FJ, Schipperen JHA. An efficient parallel procedure for the simulation of free edge delamination in composite materials. Comput Struct 2000;76(5):637–49.
[19] Riccio A, Perugini P, Scaramuzzino F. Modelling compression behaviour of delaminated composite panels. Comput Struct 2000;78(1–3):73–81.
[20] Sankar BV. A finite element for modeling delaminations in composite beams. Comput Struct 1991;38(2):239–46.
[21] Rikards R. Finite element analysis of vibration and damping of laminated composites. Compos Struct 1993; 24:193–204.
[22] Zak A, Krawczuk M, Ostachowicz W. Numerical and experimental investigation of free vibration of multi-layer delaminated composite beams and plates. Comput Mech 2000;26:309–15.
[23] Jones RM. Mechanics of composite materials. New York: McGraw-Hill Book Company; 1975.
[24] Matsunaga H. Assessment of a global higher-order deformation theory for laminated composite and sandwich plates. Compos Struct 2002;56:279–91.
[25] Bathe KJ. Finite element procedures in engineering analysis. Englewood Cliffs, NJ: Prentice-Hall; 1982.
[26] Cheng L, Nicolas J. Free vibration analysis of a cylindrical shell circular plate system with general coupling and various boundary conditions. J Sound Vib 1992;155:231–47.
[27] Cheng L. Vibroacoustic modeling of mechanically coupled structures: artificial spring technique applied to light and heavy medium. Shock Vib 1996;3:193–200.
[28] Missaoui J, Cheng L, Richard M. Free and forced vibration of a cylindrical shell with a floor partition. J Sound Vib 1996;190:21–40.
[29] Missaoui J, Cheng L. Vibroacoustic analysis of a finite cylindrical shell with a floor partition. J Sound Vib 1999; 226:101–23.
[30] Lin DX, Ni RG, Adams RD. Prediction and measurement of the vibrational damping parameters of carbon glass fiber-reinforced plastics plates. J Compos Mater 1984;18: 132–52.
[31] Yam LH, Leung TP, Li DB, et al. Theoretical and experimental study of modal strain analysis. J Sound Vib 1996;191(2):251–60.